Sub-Terahertz Metallic Multibeam Antenna Based on Sliding Aperture Technique

Lu, Hongda; Zhu, Shaoyuan; Skaik, Talal; Nie, Boyu; Liu, Yong; Wang, Yi

DOI:
10.1109/TAP.2023.3323894

Sub-Terahertz Metallic Multibeam Antenna Based on Sliding Aperture Technique

Hongda Lu, *Member, IEEE*, Shaoyuan Zhu, Talal Skaik, Boyu Nie, Yong Liu, *Member, IEEE*, and Yi Wang, *Senior Member, IEEE*

***Abstract*—This paper presents a fully metallic waveguide-based multibeam antenna operating at the band from 410 to 480 GHz. The multibeam function is achieved based on the sliding aperture technique. The antenna is composed of a beamforming network based on self-compensating waveguide phase shifters, a parallel plate waveguide (PPW) and seven waveguide feeders. Each self-compensating phase shifter is realized by equal-length widened-and-grooved waveguide sections with low-dispersion phase delay, which ensures a wide operating band. The design method of the beamforming network and the phase shifter is detailed. A prototype is manufactured using high-precision computer numerical control (CNC) machining and experimentally verified on S-parameters and radiation performances. The measured results show good impedance matching at all ports and low mutual couplings between them. The achieved beam scanning ranges within the band from 410 to 480 GHz are wider than ±30° with scan losses lower than 2.5 dB. The excellent agreement between the measured and simulated results verifies the design approach and the manufacture technique. This work demonstrates a practical solution to sub-terahertz passive multibeam antenna with a robust and reliable metallic structure.**

***Index Terms*— Sub-terahertz multibeam antenna, fully metallic antenna, sliding aperture technique, equal-length widened-and-grooved waveguide phase shifter.**

I. Introduction

Terahertz (THz)/sub-THz technology has been considered a significant potential enabler for the 6th-generation (6G) wireless communications [1], [2]. Beam steering is essential to ensure link and coverage. Active beam steering at such high frequencies faces significant technological challenges and cost barriers. As a more cost-effective solution, passive multibeam antenna technique is an attractive alternative [3]-[5] that can meet the requirement of spatial coverage with high gain in sub-THz wireless systems [6].

Two typical methods have been employed in the designs of passive multibeam antennas, based on transmission-line or quasi-optical network. These have been demonstrated at microwave and millimeter-wave bands. Examples include transmission-line networks based on Butler matrix [7]-[9] and Nolen matrix [10]-[12], and quasi-optical networks based on gradient index (GRIN) lens [13]-[18], Rotman lens [19]-[21] and reflector [22]-[24].

In recent years, several sub-THz passive multibeam antennas operating in the band above 300 GHz have been reported [25]. Most are realized in lenses. The photolithography-plasma etching technique in [26] shows its feasibility in the realization of low-loss sub-THz lens with photonic crystal waveguides in high-resistivity silicon. In [27], metallic Luneburg lens, fabricated by CNC, are directly fed by common waveguides, facilitating the interconnection with other devices. Its beam steering in E-plane relies on mechanical tilting which limits its application scenarios. [28] provides a solution to H-plane multiple beam antennas by port switching. It requires periodic posts with size less than 100 μm, making it challenging to CNC machining. A high-precision 3D printing was used. The reliability of the structure is a concern considering the fragility from the resin material as well as the large depth-width ratio of the posts. This work proposes a new antenna structure that is more friendly with CNC machining, which also overcomes the reliability issue.

Due to their low loss, manufacturability and reliability, rectangular waveguides have been a popular choice for transmission media at sub-THz bands. Various transmission lines [29], [30], filters [31]-[33], antennas [34]-[37] and other functional modules [38]-[41] have been presented. They were manufactured utilizing CNC, micromachining or high-precision 3D printing. To the best of the authors' knowledge, sub-THz multibeam antennas realized by a waveguide-based beamforming network have not been reported in the open literature. Signal distribution networks such as Butler matrix and Nolen matrix are the possible waveguide-based options. However, their complexities significantly increase when a large number of beams are required, which makes the scalability of such networks very poor.

The concept of sliding aperture multibeam antenna, with a relatively simple composition, was proposed in [42], where the complexity and scalability are not so much dependent on the number of beams. The beamforming network consists of an array of phase shifters with different phase delays. It should be noted that the realization of this concept in [42] is at 5.8 GHz based on PCB technique, which is not suitable for sub-THz band. Applying this concept to sub-THz frequencies

This work was supported by the National Natural Science Foundation of China under Grants 62271047, 61901040 and 12173006. (*Corresponding author: Hongda Lu*).

Hongda Lu, Shaoyuan Zhu, Boyu Nie and Yong Liu are with the School of Integrated Circuits and Electronics, Beijing Institute of Technology, Beijing 100081, China. (e-mail: luhongda@bit.edu.cn).

Talal Skaik and Yi Wang are with the School of Electrical Electronic and Systems Engineering, University of Birmingham, Birmingham B15 2TT, U.K.

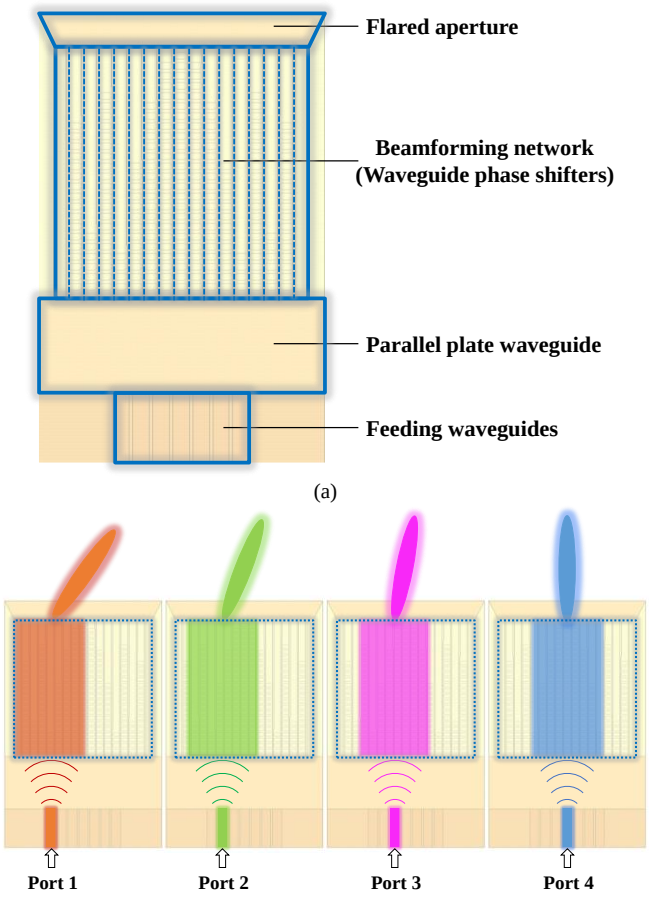

Fig. 1. (a) Diagram and (b) beam scanning principle of the waveguide-based sliding aperture multi-beam antenna (only 4 ports are shown here).

requires completely new method of phase shifter design and comprehensive investigation of the implementation.

Therefore, this paper adopts the concept of sliding aperture multibeam technique for a sub-THz antenna and proposes a novel solution of fully metallic multibeam antenna at the band above 400 GHz for the first time. Different from [42], the waveguide-based structural compositions of beamforming network and feeding network are designed. Besides, considering the fabrication feasibility at sub-THz band, the trade-off designs in the aspects such as the type of phase shifter and the maximum scanning angle have been implemented. The detailed discussions on the multibeam performances in a wideband from 410 GHz to 480 GHz are also shown in the paper. The results are experimentally verified by a CNC machined prototype.

This article is organized as follows. In section II, the basic principle and design method of the waveguide-based sub-THz sliding aperture antenna are introduced. In section III, the fabrication of the prototype, detailed measured results, discussions and comparison are given. Section IV concludes this work.

II. Antenna Design

A. Antenna principle

The multibeam antenna is composed of four parts as shown in Fig. 1(a), a beamforming network based on self-compensating waveguide phase shifter array, a parallel plate waveguide (PPW), seven feeding waveguides and a flared aperture. As seen in Fig. 1(b), the multiple beams are obtained by switching the feeding ports. Each port illuminates nearly half of the phase shifter array at a different section, which resembles an aperture sliding as a result of the changes in feeding position. In this work, the beamforming network and feeding structures are both designed based on fully metallic waveguides which can be manufactured by CNC milling at sub-THz band. The phase delays of the waveguide phase shifters are designed initially according to the requirements of the beam with the largest scanning angle, and then tuned together with the length of the PPW by considering the phase requirements of the other beams. The self-compensating phase shifters are achieved by using equal-length widened-and-grooved waveguide which provides stable phase delay over a broad band. This will be detailed later.

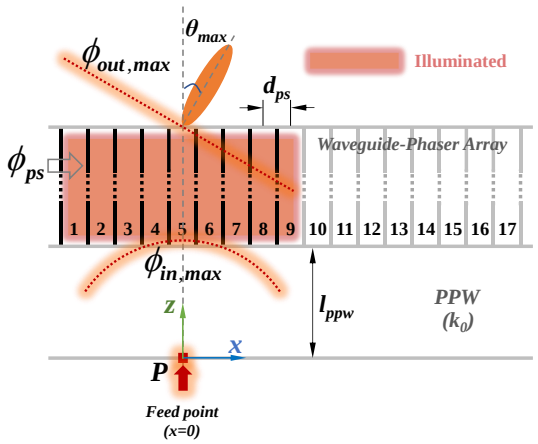

Fig. 2. Diagram of the phase shifter array and parameters for calculating phase delay at the maximum beam scanning angle.

B. Phase shifting and feed method

As proposed in [42], the phase delays of the phase shifters and the positions of the feeders are key parameters to be calculated and determined. The design method is briefed as follows, considering the characteristics of the waveguide structure.

All starts with the beam of the largest beam angle, denoted with the term '*max*'. As shown in Fig. 2, the compensating phases required from the phase shifters, ϕ_{ps}, in the left half (No. 1 to 9) of the array is the difference between the input and output phases of each waveguide, i.e. $\phi_{in,max}$ and $\phi_{out,max}$. $\phi_{in,max}$ is determined by the lateral offset, x, relative to the feed point P (where x = 0), and the length of the PPW, l_{ppw}, written as (1)

$$\phi_{in,max} = k_0 \cdot \sqrt{x^2 + l_{ppw}^2} \tag{1}$$

where k_0 is the wavenumber in the free space and the PPW. $\phi_{out,max}$ is determined by x and the maximum beam scanning angle, θ_{max}, written as (2).

$$\phi_{out,max} = k_0 \cdot x \cdot \sin\theta_{max} \tag{2}$$

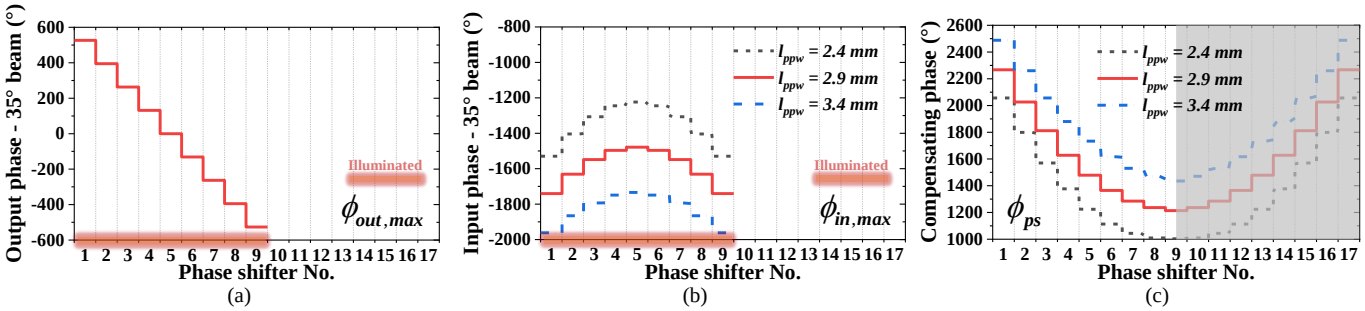

(a) (b) (c)

Fig. 3. (a) Output phases for 35° beam. (b) Input phases and (c) phase shifts when l_{ppw} = 2.4, 2.9 and 3.4 mm, respectively.

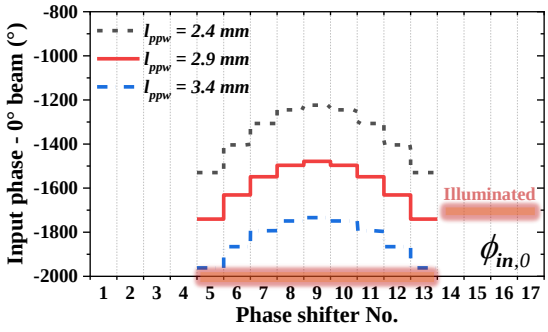

(a)

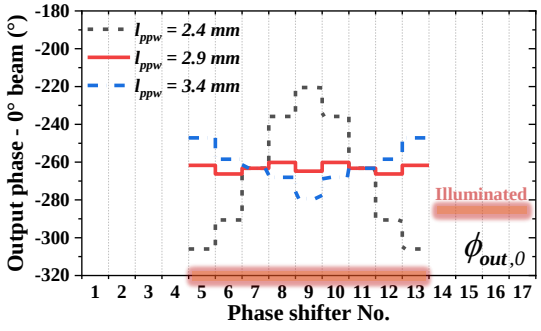

(b)

Fig. 4. (a) Input phases and (b) output phases of 0° beam when l_{ppw} = 2.4, 2.9 and 3.4 mm, respectively.

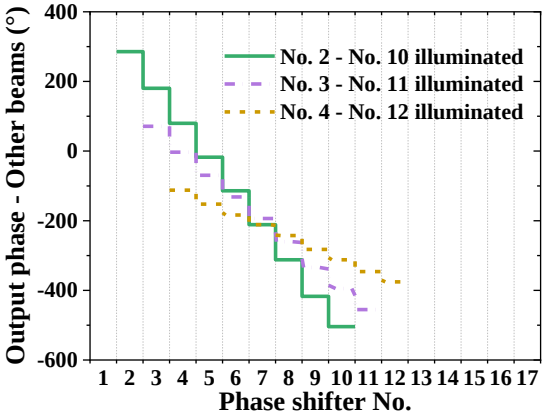

Fig. 5. Resultant output phases for other beams when phase shifters numbered 2 to 10, 3 to 11 and 4 to 12 are illuminated, respectively.

Therefore, ϕ_{ps} can be written as (3). Then, considering the symmetry of the beamforming network, the phase delays of the other half can be obtained.

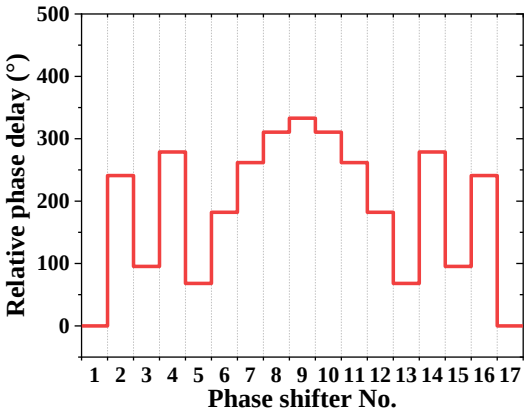

Fig. 6. Relative phase delay of each phase shifter for the entire array.

$$\phi_{ps} = \phi_{out,max} - \phi_{in,max} = k_0 \cdot \left(x \cdot \sin\theta_{max} - \sqrt{x^2 + l_{ppw}^2} \right) \quad (3)$$

It should be noted that to maximize the beam scanning range and guarantee the operating band and engineering feasibility of the waveguide-based structure, the spacing of the waveguide phase shifters, d_{ps}, is chosen as 450 μm (approximately 0.64λ at 425 GHz). This supports an expected maximum beam scanning angle of ±35° without excessive grating lobes. Now that the θ_{max} is determined to be 35° and $\phi_{out,max}$ can be obtained as shown in Fig. 3(a). According to the theory in [42], $\phi_{in,max}$ and ϕ_{ps} vary with the value of l_{ppw}, so we take the results when l_{ppw} = 2.4, 2.9 and 3.4 mm, respectively, as examples, shown in Fig. 3(b) and (c).

l_{ppw} needs to be chosen by considering the output phase requirement for the 0° beam, $\phi_{out,0}$, which can be calculated by (4)

$$\phi_{out,0} = \phi_{in,0} + \phi_{ps} \quad (4)$$

where $\phi_{in,0}$ can be easily obtained by shifting $\phi_{in,max}$ as shown in Fig. 4(a). Fig. 4(b) shows the influence of l_{ppw} on $\phi_{out,0}$. According to the results in Fig. 4, l_{ppw} is determined to be 2.9 mm as the corresponding output phases of the 0° beam show an expected uniform distribution. To further verify the effectiveness of this approach, the characteristics of the other beams are evaluated. Beams at other scanning angles with phase shifters numbered 2 to 10, 3 to 11 and 4 to 12, respectively, are illuminated in Fig. 5. They show linear wavefronts supporting different pointing angles.

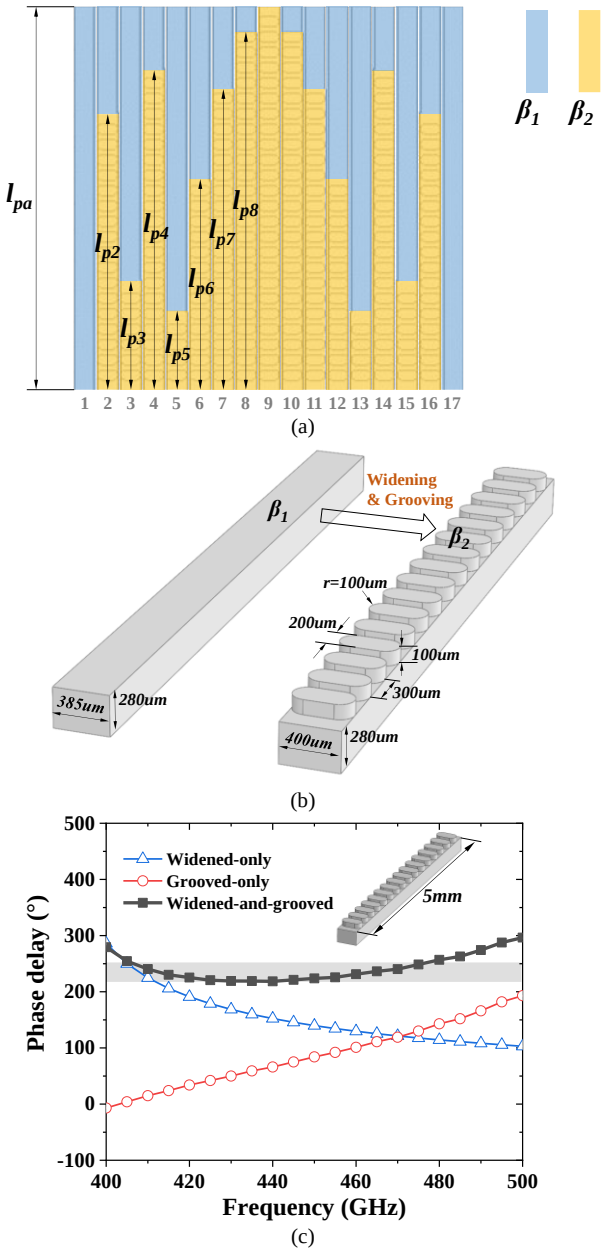

Fig. 7. (a) Diagram of the beamforming network consisting of self-compensating waveguide phase shifters. (b) Diagram of the self-compensating equal-length waveguide phase shifter and (c) phase delay performance of the phase shifter with a length of 5mm.

Finally, the phase delay of each waveguide phase shifter can be obtained. In practice, the compensating phases are wrapped to phase delays within 360°, as given in Fig. 6. These can be realized by self-compensating equal-length waveguide phase shifters will be discussed next.

C. Equal-length self-compensating waveguide phase shifters

The beamforming network is an array of waveguide phase shifters composed of two types of waveguides with phase constants of β_1 and β_2, respectively. The waveguide corresponding to β_1 is a typical rectangular waveguide with 280 μm × 385 μm section, while that corresponding to β_2 is realized by a widened-and-grooved waveguide as a self-compensating phase shifter to provide the expected phase

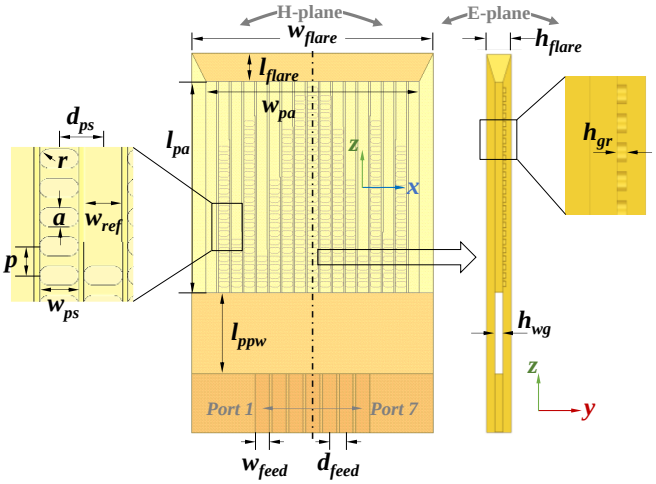

Fig. 8. Structure and detailed dimensions of the proposed antenna.

delay. As shown in Fig. 7(a), different combinations of β_1 and β_2 sections help achieve the required phase delay.

It should be noted that there have been several reported works on self-compensating phase shifters such as unequal-length unequal-width waveguide [43] and unequal-height unequal-width waveguide [44]. The equal-length widened-and-grooved self-compensating waveguide phase shifter in this paper can be treated as a specific form of the unequal-height unequal-width waveguide phase shifter. According to the theory mentioned in [44], widening and grooving a rectangular waveguide can increase the phase delays attributing to the guide wavelength change and discontinuities, respectively, but with dispersions of opposite phase slopes. Therefore, we combine these two structures to realize low-dispersion phase delay over a wide band as shown in Fig. 7(b). This type of self-compensating waveguide phase shifter was initially presented in [45] and is employed in antenna design for the first time in this paper. In addition, for the convenience of CNC machining at sub-THz band, the corners of the grooves are rounded to a radius of 0.1mm, which maintains the low-dispersion phase shifting. Fig. 7(c) illustrates the phase shifting performance of a 5 mm-long widened-and-grooved waveguide in comparison with a widened-only waveguide and a grooved-only waveguide. The dispersion is significantly suppressed by the combination of the widening and grooving. Specifically, the 5 mm-long self-compensating widened-and-grooved waveguide phase shifter provides a relative phase delay between 220° and 255° in the band from 410 to 480 GHz. It should be noted that although the discontinuities in the proposed phase shifter especially caused by the grooving bring a certain degree of reflection, the reflection coefficient level lower than -15 dB is acceptable for the antenna design in this work and can ensure a good impedance matching between the feeding waveguides and the beamforming network. To achieve the phase delay requirements shown in Fig. 6, the length parameters defined in Fig. 7(a) are determined as listed in Table I.

D. Antenna with wideband waveguide phase shifters

Based on the feeding network, the whole antenna can be

TABLE I
DIMENSIONAL PARAMETERS OF THE PROPOSED ANTENNA

Parameter	Dimension (mm)	Parameter	Dimension (mm)
w_{pa}	7.585	r	0.1
l_{pa}	5.75	h_{flare}	0.88
w_{flare}	8.585	h_{wg}	0.28
l_{flare}	1	h_{gr}	0.1
l_{ppw}	2.9	l_{p2}	4.14
w_{feed}	0.5	l_{p3}	1.64
d_{feed}	0.6	l_{p4}	4.79
d_{ps}	0.45	l_{p5}	1.17
w_{ref}	0.385	l_{p6}	3.13
w_{ps}	0.4	l_{p7}	4.5
p	0.3	l_{p8}	5.34
a	0.2		

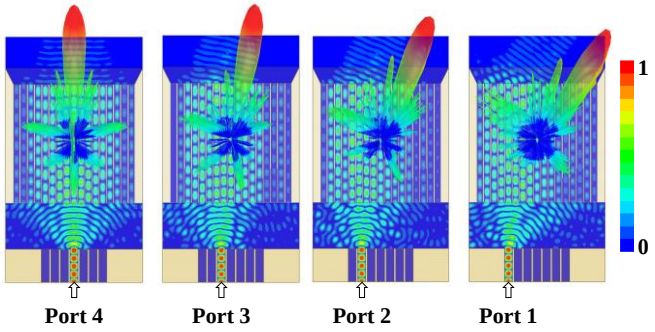

(a)

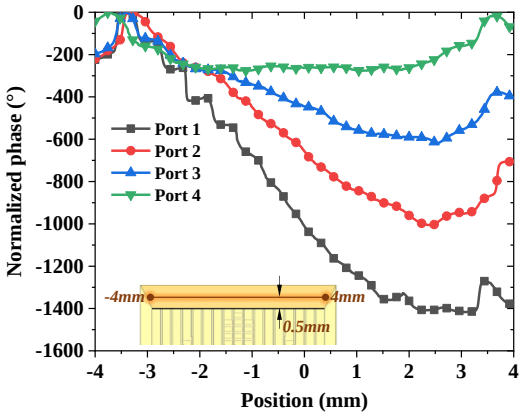

(b)

Fig. 9. Simulated (a) electric field distributions and radiation patterns of the multiple beams, and (b) the corresponding phase distributions on the radiation aperture.

obtained with dimensional parameters given in Fig. 8 and Table I. Seven rectangular waveguides are added as the multibeam feeders at the input side.

The simulated electric fields along with the radiation beams corresponding to port 1, 2, 3 and 4 are plotted in Fig. 9(a). In addition, the phase distributions on the radiation aperture are also shown in Fig. 9(b). With the switch of the feeders, the sliding of the radiation aperture is evident and the wavefronts for multiple beams are achieved.

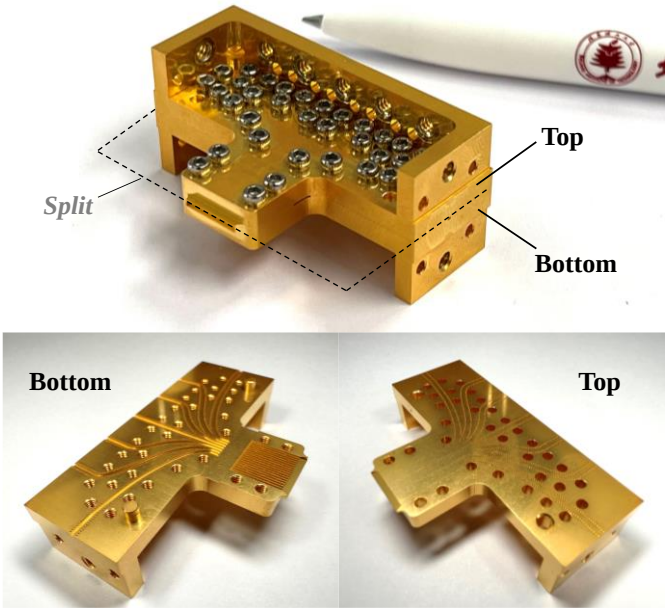

Fig. 10. Photographs of the fabricated prototype.

III. FABRICATION, RESULTS AND DISCUSSION

A. Fabrication

A prototype has been fabricated by using CNC technology. It is formed of two parts which are split along H-plane as shown in Fig. 10. To ensure the reliability of the prototype in assembly, a number of screws are employed for a secure contact between the two parts. It is also important to note that additional electromagnetic band-gap (EBG) structures, proposed in [46] and easily fabricated by using the same milling process, have been used in the feeding waveguides area to further avoid any potential leakage from the possible gap between the top and bottom parts caused by assembly error, which can be seen in Fig. 11. The example of using this kind of EBG structure to suppress wave leakage has been presented in [47]. In this work, the diameter, depth and period of the holes are 0.28, 0.21 and 0.35mm, respectively.

Fig. 11 shows the micrographs of the grooves, waveguides and holes and their key dimensions taken using Alicona optical system. Fig. 11(a) shows that in the groove and hole areas, the width accuracy is better than ±2 μm, while in the waveguide area, the width accuracy is better than ±4 μm. In addition, the measured depth of the groove is given in Fig. 11(b) which shows an error within 2 μm. The surface roughness which may lead to a degraded effective conductivity is also important for sub-THz devices. As shown in Fig. 11(c), this is better than 200 and 240 nm in the groove and waveguide, respectively, which hardly affects the device performance at this frequency band.

B. S-parameters

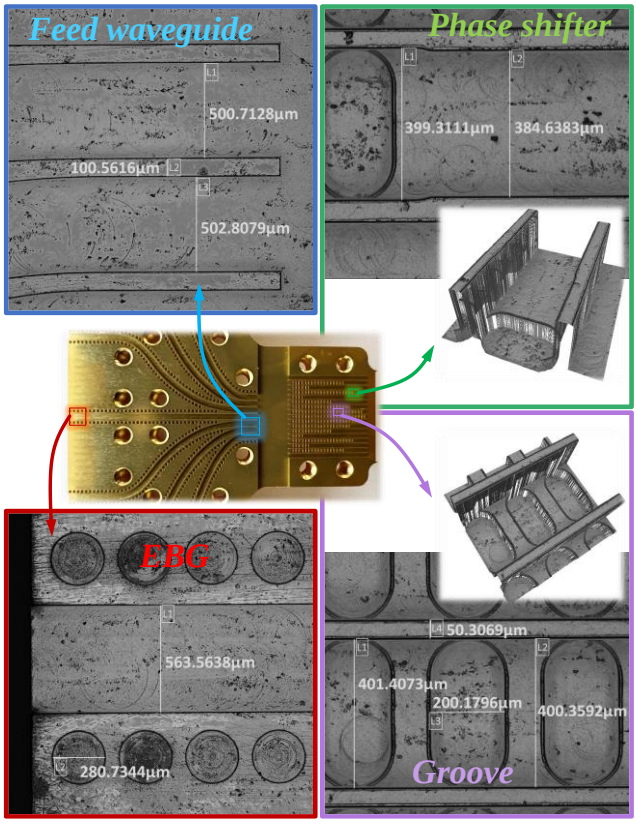

(a)

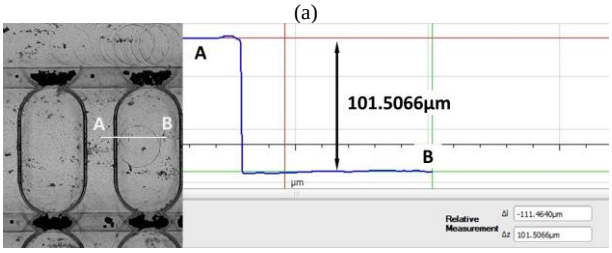

(b)

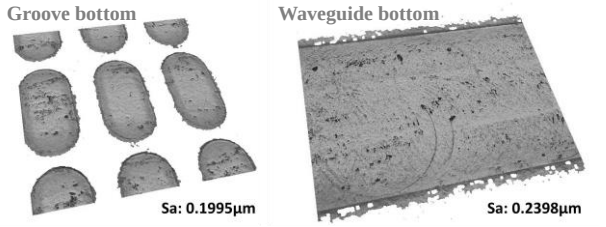

(c)

Fig. 11. Dimension and surface characterization. (a) Widths, (b) depths and (c) surface roughness of typical parts measured using Alicona optical system.

The measurement of reflection coefficients is done using a vector network analyzer (VNA) (Keysight N5247B PNA-X) with sub-THz extenders (VDI WM570, 325 to 500 GHz).

As shown in Fig. 12, the reflection coefficients at port 1, 2, 3, 5, 6, 7 are all better than -10 dB from 400 to 500 GHz. At port 4, this degrades to -8.5 dB below 420 GHz because of the superposition of the reflections at its position in the center of the feeder array. The measured results agree very well with simulation, which indicates that the proposed antenna structure can be reliably implemented by CNC. It was not possible to measure all the mutual coupling between ports due to their close proximity. The measured results for some typical

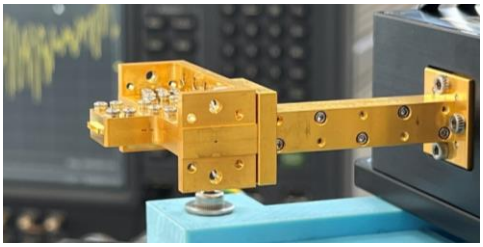

(a)

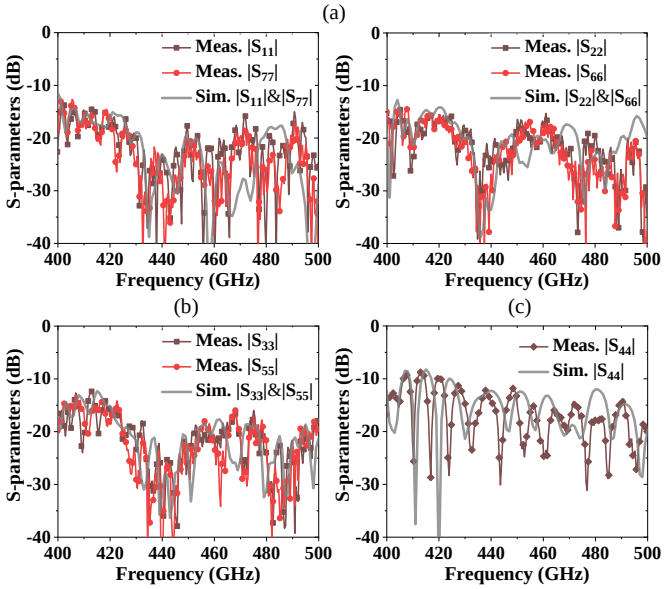

(b) (c) (d) (e)

Fig. 12. (a) Measurement setup and measured results of reflection coefficients at (b) port 1 and 7, (c) port 2 and 6, (d) port 3 and 5, and (e) port 4 in comparison with simulation.

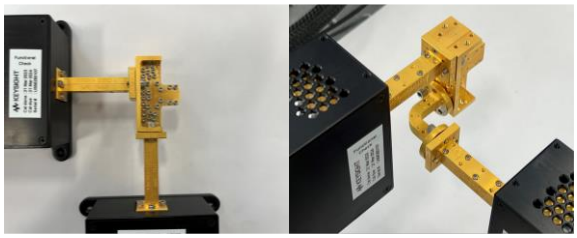

(a)

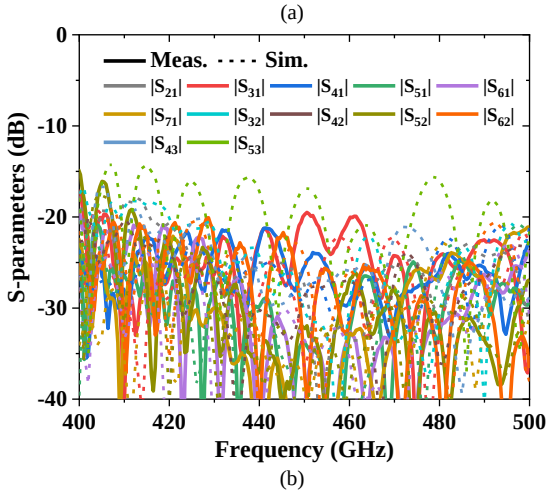

(b)

Fig. 13. (a) Measurement setup and (b) measured results of mutual couplings as compared with simulation.

ports are given in Fig. 13 together with all the simulated results. Good agreement is observed, verifying good port isolations. Overall, the mutual couplings are below -14 dB.

(a)

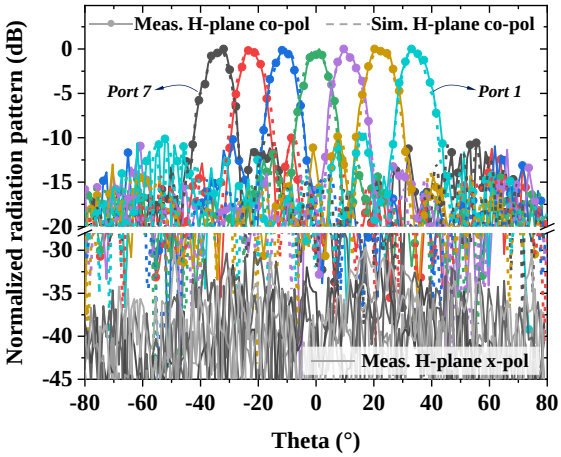

(b)

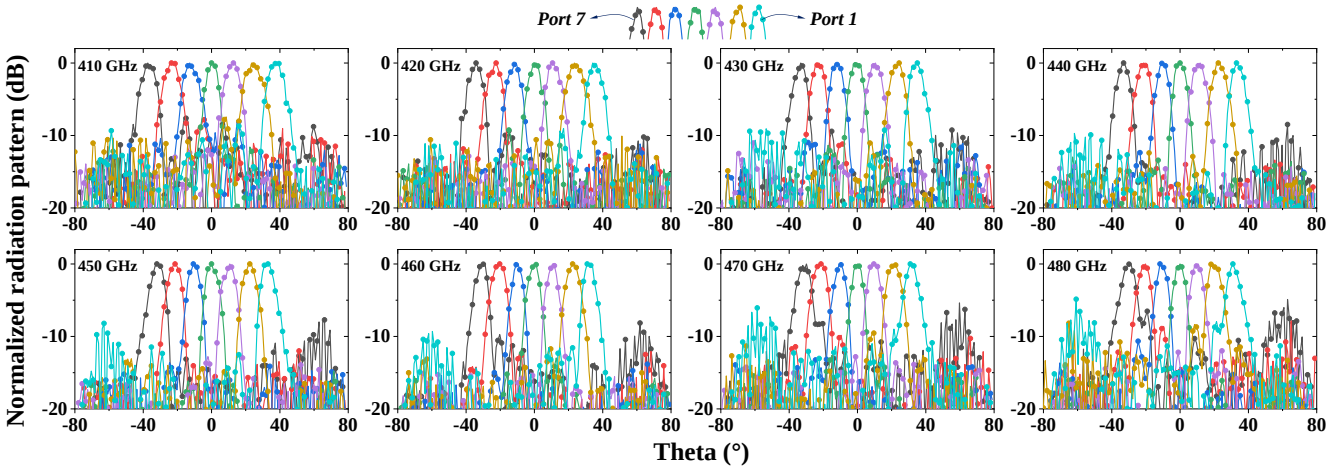

(c)

Fig. 14. (a) Measurement setup and measured H-plane multibeam radiation patterns at (b)425 GHz (compared with simulation) and (c) other frequencies from 410 to 480 GHz.

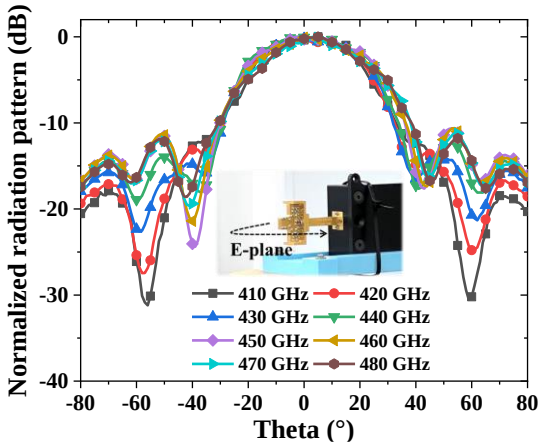

Fig. 15. Measured E-plane co-polarization radiation patterns corresponding to port 4 at frequencies from 410 to 480 GHz.

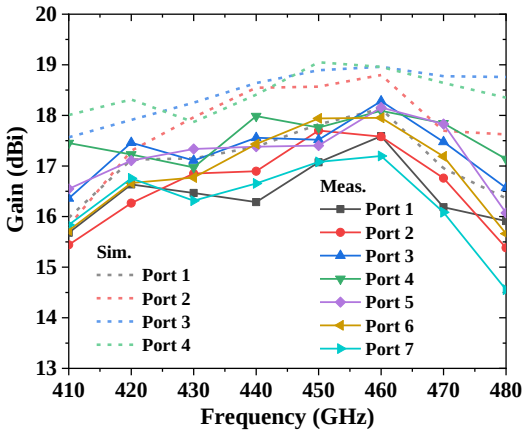

Fig. 16. Measured gains of the multiple beams corresponding to port 1 to 7 compared with simulation.

C. Radiation performances

A setup shown in Fig. 14(a) consisting of a VNA, a transmitting module, a receiving module and a rotating platform is used for the test of radiation performance.

Fig. 14(b) shows the measured co- and cross-polarization multibeam radiation patterns corresponding to the feed from port 1 to 7 at 425 GHz. The results show a beam scanning range of ±33° with a scan loss better than 1.1 dB, with a realized gain between 16.2 dBi and 17.3 dBi. The relative sidelobe levels of all the beams are lower than -10 dB. The half-power beamwidth varies from 8° to 9.5°. A good linear polarization can also be observed from the measured cross-polarization level of below -30 dB. The measured and simulated results show a good agreement.

As an evaluation of the broadband radiation performance,

TABLE II
COMPARISON WITH PREVIOUS RELATED WORKS ON TERAHERTZ MULTIBEAM ANTENNAS AND PROPOSAL OF SLIDING-APERTURE ANTENNA

Ref.	*f* (GHz)&Bandwidth	Scan range	Scan loss	Beam overlap	Multibeam principle	Network type	Fabrication
[20]	65~140(73.2%)	±30°(E-plane)	N/A	N/A	Port switch	Rotman lens	Micromachining
[26]	320~390 (19.7%)	±60°(H-plane)	N/A	<-15dB	Port switch	Luneburg lens	Silicon etching
[27]	300 (6.7%)	±25°(E-plane)	3dB	N/A	Plate tilt	Luneburg lens	CNC
[28]	355 (2.8%)	±60°(H-plane)	1.2dB	<-10dB	Port switch	Luneburg lens	3D-printing &gold-sputtering
[42]	5.5~6.1(10.3%)	±42°(H-plane)	N/A	>-4dB	Port switch	Sliding aperture	PCB
This work	**410~480 (15.7%)**	**≥ ±30°(H-plane)**	**2.5dB**	**>-5dB(425GHz) >-7dB(whole band)**	**Port switch**	**Sliding aperture**	**CNC**

the radiation patterns at other frequencies from 410 to 480 GHz have been also measured and shown in Fig. 14(c). The beam scanning ranges larger than ±30° are obtained across the band, although a slight variation between ±30° and ±36° exists as the frequency changes. It is noted that as the frequency increases to 480 GHz, some grating lobes appear higher than -10dB at the angle far away from the main lobe. This is attributed to the phase shifter spacing larger than $0.7\lambda_{480GHz}$ at 480 GHz.

The radiation patterns of the E-plane at frequencies from 410 to 480 GHz in Fig. 15 show the expected fan beams with good symmetry and a maximum radiation direction close to 0°.

The realized gains of the multiple beams have also been measured by a comparison method. As shown in Fig. 16, the scan losses within the band from 410 to 480 GHz are almost all better than 2 dB except for the result of 2.5 dB at 480 GHz.

D. Comparison

Different from [42] which proposed the concept of sliding aperture technique, this work applies a fully metallic waveguide phase shifter array to the realization of a sub-THz sliding-aperture multibeam antenna for the first time. Compared to the reported works on multibeam antennas at the band above 300 GHz in [26]-[28], this work presents a waveguide-based solution that balances the structural reliability, practicality and performance. Different from the 300 GHz fully metallic antenna in [27] that achieves multiple beams in E-plane by plate tilt, this work demonstrates a CNC manufacture solution to realizing H-plane multibeam by port switching. On the other hand, compared to the prototypes manufactured by high-resistivity silicon etching [26] and resin 3D-printing [28], the fully metallic design is structurally more robust for convenient waveguide interconnection and achieving very competitive performance. The detailed comparison is summarized in Table II.

IV. CONCLUSION

A fully metallic sub-THz waveguide-based multibeam antenna employing sliding aperture technique has been proposed and experimentally verified for the first time. Implemented using CNC machining technology, a prototype at the band from 410 to 480 GHz has been demonstrated. The measured reflection coefficients and mutual couplings are lower than -10 dB and -14 dB. The beam scanning ranges larger than ±30° and scan losses better than 2.5 dB within the operating band have been obtained. The good agreement between measured and simulated results demonstrates that the proposed antenna can be a reliable solution to sub-THz multibeam front end for high data-rate communications at the band above 400 GHz.

REFERENCES

[1] S. Dang, O. Amin, B. Shihada, and M.-S. Alouini, "What should 6G be?," *Nat. Electron.*, vol. 3, no. 1, pp. 20-29, Jan, 2020.

[2] T. S. Rappaport, Y. Xing, O. Kanhere, S. Ju, A. Madanayake, S. Mandal, A. Alkhateeb, and G. C. Trichopoulos, "Wireless Communications and Applications Above 100 GHz: Opportunities and Challenges for 6G and Beyond," *IEEE Access*, vol. 7, pp. 78729-78757, Jun, 2019.

[3] W. Hong, Z. H. Jiang, C. Yu, J. Zhou, P. Chen, Z. Yu, H. Zhang, B. Yang, X. Pang, M. Jiang, Y. Cheng, M. K. T. Al-Nuaimi, Y. Zhang, J. Chen, and S. He, "Multibeam Antenna Technologies for 5G Wireless Communications," *IEEE Trans. Antennas Propag.*, vol. 65, no. 12, pp. 6231-6249, Dec, 2017.

[4] W. Hong, Z. H. Jiang, C. Yu, D. Hou, H. Wang, C. Guo, Y. Hu, L. Kuai, Y. Yu, Z. Jiang, Z. Chen, J. Chen, Z. Yu, J. Zhai, N. Zhang, L. Tian, F. Wu, G. Yang, Z. C. Hao, and J. Y. Zhou, "The Role of Millimeter-Wave Technologies in 5G/6G Wireless Communications," *IEEE Journal of Microwaves*, vol. 1, no. 1, pp. 101-122, Jan, 2021.

[5] Y. J. Guo, M. Ansari, and N. J. G. Fonseca, "Circuit Type Multiple Beamforming Networks for Antenna Arrays in 5G and 6G Terrestrial and Non-Terrestrial Networks," *IEEE Journal of Microwaves*, vol. 1, no. 3, pp. 704-722, Jul, 2021.

[6] Y. J. Guo, M. Ansari, R. W. Ziolkowski, and N. J. G. Fonseca, "Quasi-Optical Multi-Beam Antenna Technologies for B5G and 6G mmWave and THz Networks: A Review," *IEEE Open Journal of Antennas and Propagation*, vol. 2, pp. 807-830, Jul, 2021.

[7] Q. Wu, J. Hirokawa, J. Yin, C. Yu, H. Wang, and W. Hong, "Millimeter-Wave Multibeam Endfire Dual-Circularly Polarized Antenna Array for 5G Wireless Applications," *IEEE Trans. Antennas Propag.*, vol. 66, no. 9, pp. 4930-4935, Sep, 2018.

[8] N. Ashraf, A. R. Sebak, and A. A. Kishk, "PMC Packaged Single-Substrate 4 × 4 Butler Matrix and Double-Ridge Gap Waveguide Horn Antenna Array for Multibeam Applications," *IEEE Trans. Microw. Theory Techn.*, vol. 69, no. 1, pp. 248-261, Jan, 2021.

[9] Y. Li, and K. Luk, "A Multibeam End-Fire Magnetoelectric Dipole Antenna Array for Millimeter-Wave Applications," *IEEE Trans. Antennas Propag.*, vol. 64, no. 7, pp. 2894-2904, Jul, 2016.

[10] T. Djerafi, N. J. G. Fonseca, and K. Wu, "Planar Ku-Band 4 × 4 Nolen Matrix in SIW Technology," *IEEE Trans. Microw. Theory Techn.*, vol. 58, no. 2, pp. 259-266, Feb, 2010.

[11] C. A. Guo, Y. J. Guo, H. Zhu, W. Ni, and J. Yuan, "Optimization of Multibeam Antennas Employing Generalized Joined Coupler Matrix," *IEEE Trans. Antennas Propag.*, vol. 71, no. 1, pp. 215-224, Jan, 2023.

[12]H. Zhu, M. Ansari, and Y. J. Guo, "Wideband Beam-Forming Networks Utilizing Planar Hybrid Couplers and Phase Shifters," *IEEE Trans. Antennas Propag.*, vol. 70, no. 9, pp. 7592-7602, Sep, 2022.

[13]J. Liu, H. Lu, Z. Dong, Z. Liu, Y. Liu, and X. Lv, "Fully Metallic Dual-Polarized Luneburg Lens Antenna Based on Gradient Parallel Plate Waveguide Loaded With Nonuniform Nail," *IEEE Trans. Antennas Propag.*, vol. 70, no. 1, pp. 697-701, Jan, 2022.

[14]Y. Su, and Z. N. Chen, "A Radial Transformation-Optics Mapping for Flat Ultra-Wide-Angle Dual-Polarized Stacked GRIN MTM Luneburg Lens Antenna," *IEEE Trans. Antennas Propag.*, vol. 67, no. 5, pp. 2961-2970, May, 2019.

[15]O. Quevedo-Teruel, J. Miao, M. Mattsson, A. Algaba-Brazalez, M. Johansson, and L. Manholm, "Glide-Symmetric Fully Metallic Luneburg Lens for 5G Communications at Ka-Band," *IEEE Antennas Wireless Propag. Lett.*, vol. 17, no. 9, pp. 1588-1592, Sep, 2018.

[16]H. Lu, Z. Liu, Y. Liu, H. Ni, and X. Lv, "Compact Air-Filled Luneburg Lens Antennas Based on Almost-Parallel Plate Waveguide Loaded With Equal-Sized Metallic Posts," *IEEE Trans. Antennas Propag.*, vol. 67, no. 11, pp. 6829-6838, Nov, 2019.

[17]Z. Qu, S. W. Qu, Z. Zhang, S. Yang, and C. H. Chan, "Wide-Angle Scanning Lens Fed by Small-Scale Antenna Array for 5G in Millimeter-Wave Band," *IEEE Trans. Antennas Propag.*, vol. 68, no. 5, pp. 3635-3643, May, 2020.

[18]S. Yang, Q. Chen, F. Mesa, N. J. G. Fonseca, and O. Quevedo-Teruel, "Geodesic Half-Maxwell Fish-Eye-Lens Antenna," *IEEE Trans. Antennas Propag.*, vol. 71, no. 3, pp. 2330-2338, Mar, 2023.

[19]Y. J. Cheng, W. Hong, K. Wu, Z. Q. Kuai, C. Yu, J. X. Chen, J. Y. Zhou, and H. J. Tang, "Substrate Integrated Waveguide (SIW) Rotman Lens and Its Ka-Band Multibeam Array Antenna Applications," *IEEE Trans. Antennas Propag.*, vol. 56, no. 8, pp. 2504-2513, Aug, 2008.

[20]N. Jastram, and D. S. Filipovic, "Design of a Wideband Millimeter Wave Micromachined Rotman Lens," *IEEE Trans. Antennas Propag.*, vol. 63, no. 6, pp. 2790-2796, 2015.

[21]J. Li, C. He, H. Fan, and R. Jin, "Gain-Equalized Multibeam Antenna Fed by a Compact Dual-Layer Rotman Lens at Ka-Band," *IEEE Trans. Antennas Propag.*, vol. 70, no. 3, pp. 2307-2311, Mar, 2022.

[22]Y. J. Cheng, W. Hong, and K. Wu, "Millimeter-Wave Substrate Integrated Waveguide Multibeam Antenna Based on the Parabolic Reflector Principle," *IEEE Trans. Antennas Propag.*, vol. 56, no. 9, pp. 3055-3058, Sep, 2008.

[23]Y. Bi, Y. Li, and J. Wang, "3-D Printed Wideband Cassegrain Antenna With a Concave Subreflector for 5G Millimeter-Wave 2-D Multibeam Applications," *IEEE Trans. Antennas Propag.*, vol. 68, no. 6, pp. 4362-4371, Jun, 2020.

[24]H. Li, C. Li, S. Zheng, H. Gao, and G. Fang, "Design of a Multiple-Beam Cassegrain Antenna With Quasi-Optical Isolator at 200 GHz for Target Tracking," *IEEE Antennas Wireless Propag. Lett.*, vol. 19, no. 10, pp. 1779-1783, Oct, 2020.

[25]X. Fu, F. Yang, C. Liu, X. Wu, and T. J. Cui, "Terahertz Beam Steering Technologies: From Phased Arrays to Field-Programmable Metasurfaces," *Advanced Optical Materials*, vol. 8, no. 3, pp. 1900628, Aug, 2020.

[26]D. Headland, W. Withayachumnankul, R. Yamada, M. Fujita, and T. Nagatsuma, "Terahertz multi-beam antenna using photonic crystal waveguide and Luneburg lens," *APL Photonics*, vol. 3, no. 12, pp. 126105:1-126105:18, Dec, 2018.

[27]K. Sato, and Y. Monnai, "Terahertz Beam Steering Based on Trajectory Deflection in Dielectric-Free Luneburg Lens," *IEEE Trans. THz Sci. Technol.*, vol. 10, no. 3, pp. 229-236, May, 2020.

[28]B. Nie, H. Lu, T. Skaik, Y. Liu, and Y. Wang, "A 3D-Printed Subterahertz Metallic Surface-Wave Luneburg Lens Multibeam Antenna," *IEEE Trans. THz Sci. Technol.*, vol. 13, no. 3, pp. 297-301, May, 2023.

[29]B. Beuerle, J. Campion, U. Shah, and J. Oberhammer, "A Very Low Loss 220–325 GHz Silicon Micromachined Waveguide Technology," *IEEE Trans. THz Sci. Technol.*, vol. 8, no. 2, pp. 248-250, Mar, 2018.

[30]X. Shang, M. Ke, Y. Wang, and M. J. Lancaster, "WR-3 Band Waveguides and Filters Fabricated Using SU8 Photoresist Micromachining Technology," *IEEE Trans. THz Sci. Technol.*, vol. 2, no. 6, pp. 629-637, Nov, 2012.

[31]O. Glubokov, X. Zhao, J. Campion, U. Shah, and J. Oberhammer, "Micromachined Filters at 450 GHz With 1% Fractional Bandwidth and Unloaded Q Beyond 700," *IEEE Trans. THz Sci. Technol.*, vol. 9, no. 1, pp. 106-108, Jan, 2019.

[32]J. Zhuang, Z. Hao, and W. Hong, "Silicon Micromachined Terahertz Bandpass Filter With Elliptic Cavities," *IEEE Trans. THz Sci. Technol.*, vol. 5, no. 6, pp. 1040-1047, Nov, 2015.

[33]T. Skaik, Y. Wang, M. Salek, P. Hunyor, H. Wang, P. G. Huggard, T. Starke, M. Attallah, and R. Martinez, "A 3-D Printed 300 GHz Waveguide Cavity Filter by Micro Laser Sintering," *IEEE Trans. THz Sci. Technol.*, vol. 12, no. 3, pp. 274-281, May, 2022.

[34]J. Hu, W. T. Lv, H. T. Zhu, Z. Lou, D. Liu, J. Q. Ding, and S. C. Shi, "Design, Uncertainty Analysis, and Measurement of a Silicon-Based Platelet THz Corrugated Horn," *IEEE Trans. Antennas Propag.*, vol. 70, no. 7, pp. 5897-5901, Jul, 2022.

[35]A. Gomez-Torrent, T. Tomura, W. Kuramoto, J. Hirokawa, I. Watanabe, A. Kasamatsu, and J. Oberhammer, "A 38 dB Gain, Low-Loss, Flat Array Antenna for 320–400 GHz Enabled by Silicon-on-Insulator Micromachining," *IEEE Trans. Antennas Propag.*, vol. 68, no. 6, pp. 4450-4458, Jun, 2020.

[36]L. Chang, Y. Li, Z. Zhang, S. Wang, and Z. Feng, "Planar Air-Filled Terahertz Antenna Array Based on Channelized Coplanar Waveguide Using Hierarchical Silicon Bulk Micromachining," *IEEE Trans. Antennas Propag.*, vol. 66, no. 10, pp. 5318-5325, Oct, 2018.

[37]B. Zhang, Z. Zhan, Y. Cao, H. Gulan, P. Linnér, J. Sun, T. Zwick, and H. Zirath, "Metallic 3-D Printed Antennas for Millimeter- and Submillimeter Wave Applications," *IEEE Trans. THz Sci. Technol.*, vol. 6, no. 4, pp. 592-600, Jul, 2016.

[38]A. Gomez-Torrent, U. Shah, and J. Oberhammer, "Compact Silicon-Micromachined Wideband 220–330-GHz Turnstile Orthomode Transducer," *IEEE Trans. THz Sci. Technol.*, vol. 9, no. 1, pp. 38-46, Jan, 2019.

[39]G. Chattopadhyay, T. Reck, C. Lee, and C. Jung-Kubiak, "Micromachined Packaging for Terahertz Systems," *Proc. IEEE*, vol. 105, no. 6, pp. 1139-1150, Jun, 2017.

[40]A. Khudchenko, R. Hesper, A. M. Baryshev, J. Barkhof, K. Rudakov, D. Montofré, D. v. Nguyen, V. P. Koshelets, P. N. Dmitriev, M. Fominsky, C. Heiter, S. Heyminck, R. Güsten, and B. Klein, "Design and Performance of a Sideband Separating SIS Mixer for 800–950 GHz," *IEEE Trans. THz Sci. Technol.*, vol. 9, no. 6, pp. 532-539, Nov, 2019.

[41]H. Lu, Z. Liu, P. Zhao, Y. Liu, and X. Lv, "Experimental Realization of Silicon Micromachined Terahertz Diplexer-Antenna Module for Heterodyne Receiver," *IEEE Trans. Antennas Propag.*, vol. 70, no. 8, pp. 7130-7135, Aug, 2022.

[42]Y. Hou, L. Chang, Y. Li, Z. Zhang, and Z. Feng, "Linear Multibeam Transmitarray Based on the Sliding Aperture Technique," *IEEE Trans. Antennas Propag.*, vol. 66, no. 8, pp. 3948-3958, Aug, 2018.

[43]Y. J. Cheng, W. Hong, and K. Wu, "Broadband Self-Compensating Phase Shifter Combining Delay Line and Equal-Length Unequal-Width Phaser," *IEEE Trans. Microw. Theory Techn.*, vol. 58, no. 1, pp. 203-210, Jan, 2010.

[44]J. Deng, P. Burasa, and K. Wu, "Compact 140–220 GHz E/H Waveguide Phase Shifter and Its Application to Terahertz Multiport Circuits," *IEEE Trans. THz Sci. Technol.*, vol. 13, no. 5, pp. 511-525, Sep, 2023.

[45]Z. Liu, J. Liu, H. Lu, Y. Liu, and X. Lv, "Terahertz Broadband Self-Compensating Waveguide Phase Shifter," in *2019 International Symposium on Antennas and Propagation (ISAP)*, 2019, pp. 1-3.

[46]M. Ebrahimpouri, E. Rajo-Iglesias, Z. Sipus, and O. Quevedo-Teruel, "Cost-Effective Gap Waveguide Technology Based on Glide-Symmetric Holey EBG Structures," *IEEE Trans. Microw. Theory Techn.*, vol. 66, no. 2, pp. 927-934, Feb, 2018.

[47]O. Zetterstrom, M. Petek, P. Castillo-Tapia, P.-C. Á, N. J. G. Fonseca, and O. Quevedo-Teruel, "V-Band Fully Metallic Geodesic Luneburg Lens Antenna," *IEEE Trans. Antennas Propag.*, vol. 71, no. 2, pp. 1965-1970, Feb, 2023.